micrographs of the ϵ_M and α_M phases respectively.

Fig. 2a is a bright-field micrograph of a HIDT region which formed along a $\{1\,1\,1\}_\gamma$ plane parallel to the annealing twin boundary A–A′. The bands in the HIDT region and parallel to A–A′ are the deformation twins and the fine, closely spaced line structures crossing the banded regions are ϵ_M. As was common for well developed HIDT regions, a crack was observed along the general direction of the deformation twins. Fig. 2b is an electron diffraction pattern from area B of Fig. 2a. From interplanar spacings [9] obtained from the radii of circles drawn through the various groups of diffraction spots in Fig. 2b, both deformation twins and ϵ_M are present in the HIDT region. The ϵ_M visible in the dark-field micrograph of Fig. 2c again consists of a fine, closely spaced line structure. Fig. 2d is a dark-field micrograph which shows some of the deformation twinned regions.

Since the microstructure and the deformation-fracture process of the HIDT regions are similar to those of the strain-induced deformation twinned regions [2–5] and since HIDT was not found in bulk TEM specimens thinned finally after cathodic charging, HIDT appears to be a thin-foil phenomena. However, in addition to the unique presence of the associated hydrogen-induced martensitic phases, the HIDT regions were usually composed of several individual deformation twins ranging from 250 to 500 Å in width. This contrasts with the strain-induced deformation twin regions which were apparently composed of a single wide twin.

References

1. S. MAHAGAN and D. F. WILLIAMS, *Int. Met. Rev.* 18 (1973) 43.
2. J. W. MATTHEWS, *Acta. Met.* 18 (1970) 175.
3. R. E. WINTER and J. E. FIELD, *Phil. Mag.* 29 (1974) 395.
4. S. MARUYAMA and H. KIHO, "Electron Microscopy: Sixth International Congress for Electron Microscopy", Vol. 1 (Maruzen, Kyoto, 1966) p. 311.
5. A. CATLIN, W. P. WALKER, K. R. LAWLESS, *Acta. Met.* 8 (1960) 734.
6. C. K. H. DUBOSE and J. O. STIEGLER, *Rev. Sci. Instrum.* 38 (1967) 694.
7. R. LAGNEBORG, *Acta. Met.* 12 (1964) 823.
8. H. FUJITA, and S. UEDA, *ibid.* 20 (1972) 759.
9. M. L. HOLZWORTH and M. R. LOUTHAM, JUN., *Corrosion* 24 (1968) 110.

Received 21 June
and accepted 19 July 1976

J. M. RIGSBEE*
Department of Metallurgical Engineering, Michigan Technological University, Houghton, Michigan, USA
R. B. BENSON, JUN.
Department of Materials Engineering, North Carolina State University, Rayleigh, North Carolina, USA

*Present address: Republic Steel Research Center, 6801 Brecksville Road, Cleveland, Ohio, USA

Growth of oxide in situ composites: the systems lithium ferrite–lithium niobate, lithium ferrite–lithium tantalate, and nickel ferrite–barium titanate

The general utility of capillary shaping techniques were recently evaluated [1–4] for growing ceramic *in situ* composites [4] to be used in non-structural applications. During these studies we identified three new oxide-phase systems for which directional freezing produces well-aligned composite microstructures: lithium ferrite–lithium niobate, lithium ferrite–lithium tantalate, and nickel ferrite–barium titanate. The melting relations for these systems and the morphological characteristics of the directionally frozen composites are reported here.

Often the phase relations for attractive ternary and higher order oxide systems are too fragmentary or imprecisely known to select melt compositions for composite growth. Therefore, we melted and cast representative compositions from candidate systems and searched the specimen microstructures for morphologically uncomplicated two-phase aggregates. Three systems, $Li_{0.5}Fe_{2.5}O_4$–$LiNbO_3$, $Li_{0.5}Fe_{2.5}O_4$–$LiTaO_3$, and $NiFe_2O_4$–$BaTiO_3$, yielded promising microstructures; for these systems partial phase diagrams were constructed from cooling curves, X-ray diffraction and microstructural data.

The cooling curves were developed by monitoring the output of a Pt/Pt–6% Rh thermocouple immersed in 40 g charges of each oxide melt. The temperature was cycled several times through the

freezing point using a variety of heating and cooling rates. Debye–Scherrer X-ray diffraction patterns (Cu$K\alpha$, Ni filter) were obtained on powdered samples of each composition via a standard 114.59 mm diameter camera.

For microstructural evaluation the oxide specimens were mounted in a thermosetting resin, lapped flat with alumina grit and polished with Syton®* on a Politex D pad.

For each system we investigated, the liquid oxides readily wetted platinum shaping dies so that no external pressure was required for die filling as in Stepanov's method [1]. Our growth technique thus closely resembled the edge-defined film-fed growth method in which the oxide liquid is carried by surface tension forces to the die top via a capillary passage [4]. The freezing solid is extracted from the liquid layer on the die surface by inserting a seed and withdrawing it upwards.

The die geometries we used for composite growth were: (1) a rectangular platinum die 25 mm deep by 6 mm wide comprised of two blades 1.25 mm thick with a 0.8 mm capillary gap, and (2) a cylindrical die, 25 mm deep by 6 mm o.d., having a central 0.8 mm feed hole and three peripheral 0.8 mm holes (Fig. 1). As illustrated in the figure, the dies were welded to the crucible walls with platinum arms. During growth runs the platinum crucible was inserted in a zirconia crucible for insulation.

From the phase diagrams for each candidate system, the minimum melting composition was chosen for growth. The oxide components (see Table I) weighed on an analytical balance to the growth composition, were blended for several hours, then melted down in the platinum crucible with the die in place. The liquids were homogenized in air for several hours, then growth was initiated on a platinum wire, or in some cases an $LiNbO_3$ single crystal seed. Samples up to 200 mm long were grown in this way at rates ranging from 0.1 to 2 cm h^{-1}.

The lithium ferrite–lithium niobate system is apparently pseudobinary in character displaying a eutectic at 18 mol% $Li_{0.5}Fe_{2.5}O_4$ and 1180° C (Fig. 2). Only the primary phases were ever observed in the microstructures of specimens cast at various compositions across the system. Nor was

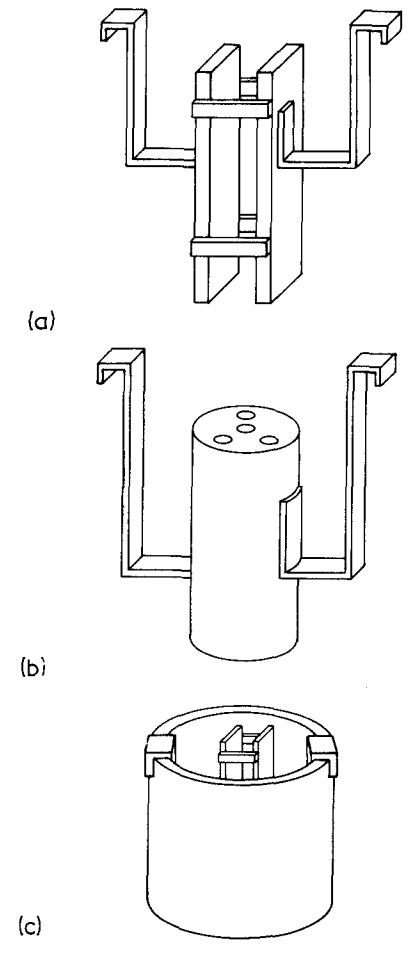

Figure 1 Platinum dies used for EFG growth of composites: (a) rectangular, (b) cylindrical, (c) rectangular die mounted in crucible.

any evidence for extraneous phases evident in the Debye–Scherrer X-ray diffraction patterns. The unit cell dimensions measured on specimens of the composite quenched from the melting temperature agree closely (± 0.001 Å) with those of the pure

TABLE I Raw materials for composite growth studies

Material	Supplier	Purity or grade
Li_2CO_3	Johnson–Matthey Puratronic	Grade I
Nb_2O_5	Johnson–Matthey Puratronic	Grade I
Fe_2O_3	Johnson–Matthey Puratronic	Grade I
TiO_2	A. D. Mackay, Inc	99.95%
$BaCO_3$	Mallinckrodt	S.L. Grade
NiO	Baker, Ultrex	99.999%
Ta_2O_5	Kennametal	99.95%

*Trademark Monsanto Chemical Co.

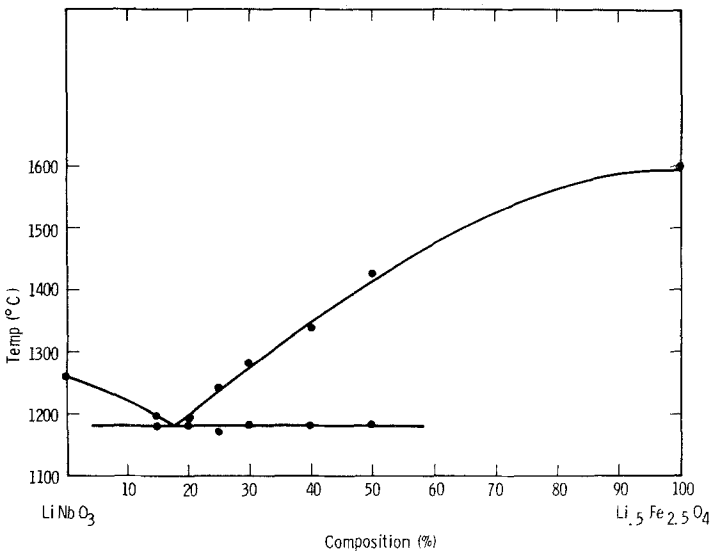

Figure 2 Partial phase diagram for the system $Li_{0.5}Fe_{2.5}O_4$–$LiNbO_3$.

phases $LiNbO_3$, $a = 5.149$ Å, $c = 13.862$ Å [5], and $Li_{0.5}Fe_{2.5}O_4$, $a = 8.333$ Å [6], suggesting that solid solution in the terminal phases is small or absent.

Lithium ferrite–niobate composites grown from both round and rectangular dies showed the same general features. Over most of the ingot's cross-section the microstructure consists of parallel lithium ferrite blades distributed in a lithium niobate matrix (Fig. 3). At rates below 0.2 cm h^{-1} the blades became increasingly irregular developing evident lateral facets (Fig. 4). In contrast, as the growth rate was raised above 1.6 cm h^{-1}, the ferrite phase tended to form rods, a fact in keeping with its rather low volume fraction, ~ 15%.

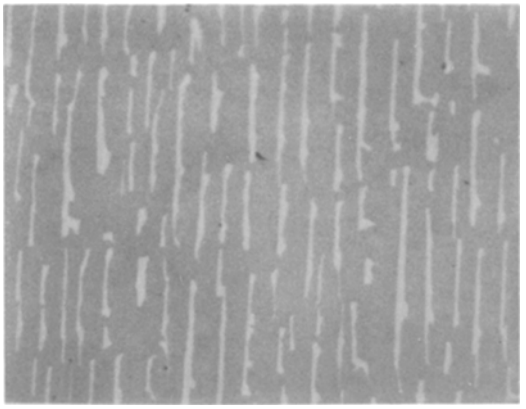

Figure 3 Blade type microstructure of the $Li_{0.5}Fe_{2.5}O_4$–$LiNbO_3$ composite directionally frozen at 0.4 cm h^{-1}. Transverse section × 262.5

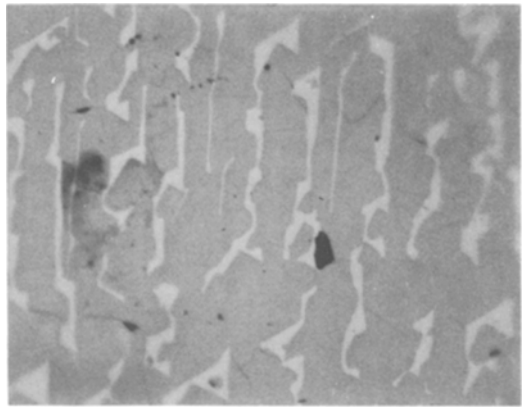

Figure 4 Faceted ferrite blades formed in a $Li_{0.5}Fe_{2.5}O_4$–$LiNbO_3$ composite directionally frozen at 0.2 cm h^{-1}. Transverse section × 262.5

The ferrite phase aligns preferentially normal to the solid–liquid interface except in the vicinity of the die periphery. There the solid–liquid interface becomes sharply convex to the liquid and microstructural alignment is lost. Over the limited range of growth rates (R) that we studied, the blade spacing (λ) of the aligned material varies as $R^{-1/2}$ in the fashion typical of other *in situ* composites [2] (Fig. 5).

Although it is not evident in Figs. 3 and 4, we often observed cracks running between and sometimes through the ferrite blades. Fracture apparently initiated due to the differential contraction between the phases on cooling from the growth temperature. The preferential alignment of the

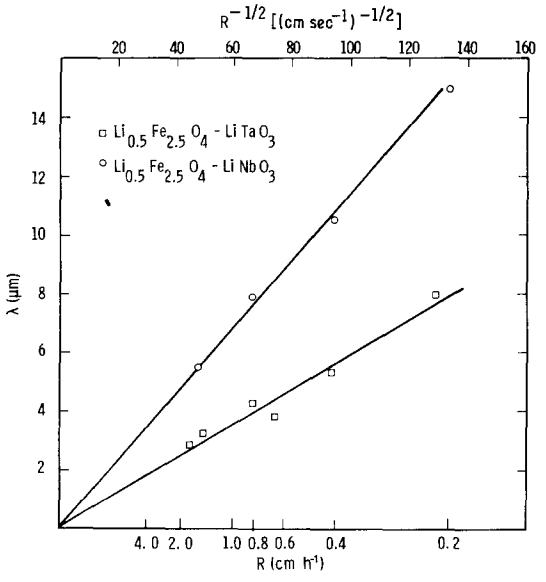

Figure 5 Variation in interphase spacing, λ, with freezing rate, R, for directionally frozen lithium ferrite–lithium niobate and lithium ferrite–lithium tantalate composites.

cracks in specific matrix directions suggests that cleavage through the niobate phase is a favoured fracture mechanism.

As with the lithium ferrite–niobate system, the lithium ferrite–tantalate system is pseudobinary but with the eutectic point shifted to 44 mol% lithium ferrite and 1345° C (Fig. 6). The shift of the eutectic point to higher temperature and higher ferrite composition is anticipated from the higher fusion temperature of $LiTaO_3$, 1650° C, compared to $LiNbO_3$, 1260° C. The cell dimensions for the composite phases again closely approximated those of the pure end members, $LiTaO_3$, $a = 5.159$ Å, $c = 13.76$ Å [7], and $Li_{0.5}Fe_{2.5}O_4$, $a = 8.333$ Å.

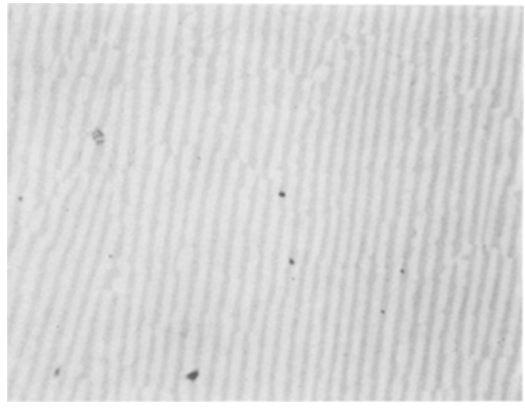

Figure 7 Lamellar structure in $Li_{0.5}Fe_{2.5}O_4$–$LiTaO_3$ composite directionally frozen at 0.2 cm h^{-1}. Transverse section × 262.5

With the shift in eutectic temperature toward an equimolar ferrite–tantalate ratio, the volumetric ratio of the phases approaches one and the composite microstructure becomes almost a classic lamellar distribution (Fig. 7). As the freezing rate is raised to 2 cm h^{-1}, however, the lamellar structure breaks down into eutectic colonies [8] elongated parallel to the lamellar planes (Fig. 8). The interphase spacing of the composite again varies approximately with $R^{-1/2}$ (Fig. 5).

Cracking is much less prevalent in the ferrite–

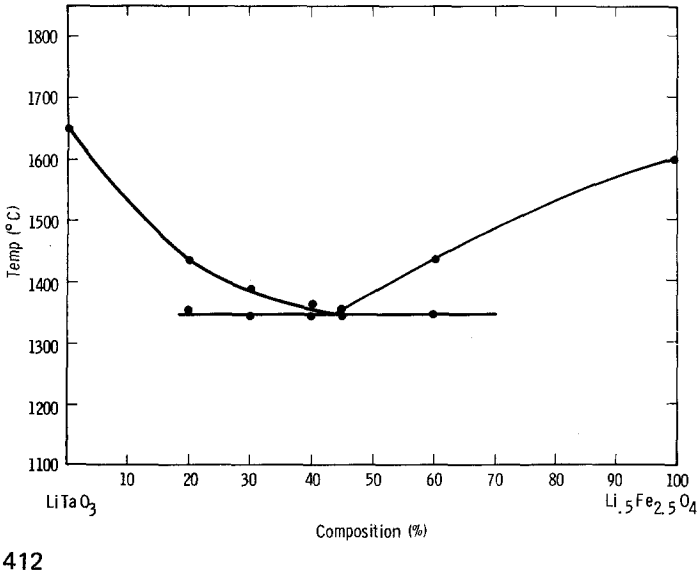

Figure 6 Partial phase diagram for the system $Li_{0.5}Fe_{2.5}O_4$–$LiTaO_3$.

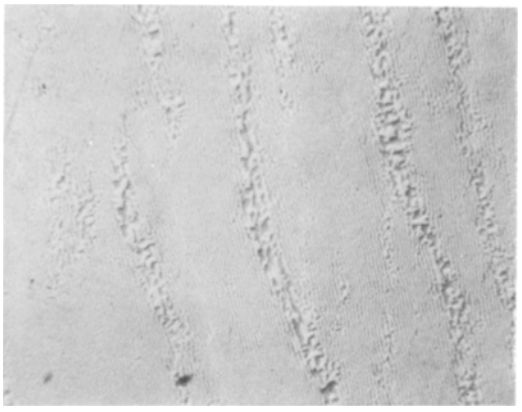

Figure 8 Colony structure formed at 2 cm h^{-1} in a $Li_{0.5}Fe_{2.5}O_4$–$LiTaO_3$ composite.

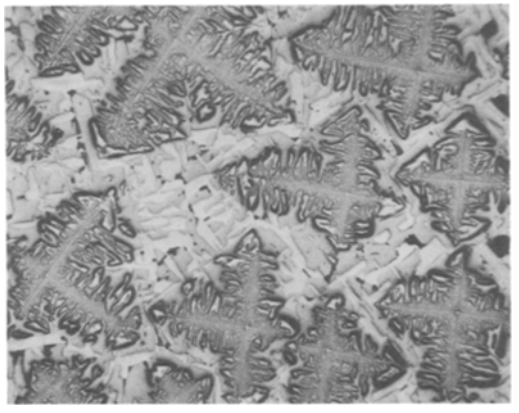

Figure 10 Four-fold spinel dendrites with interdendritic eutectic formed by directionally freezing a nickel ferrite–barium titanate composite at 0.4 cm h^{-1}. Transverse section × 52.5

tantalate composites than in those formed from ferrite and niobate. When present, the cracks propagate through both ferrite and tantalate phases in a random fashion rather than along cleavage planes.

Our cooling curve data for the nickel ferrite–barium titanate system show considerable scatter (Fig. 9). Although X-ray patterns from the solidified samples indicate only the ferrite, $a = 8.339$ Å [9], and titanate, $a = 3.994$ Å, $c = 4.038$ Å [10] phases are present, the microstructural evidence described below strongly suggests that the system is not pseudobinary. Instead, the liquidus curve we determined simply represents a minimum on the particular composition join in the quaternary system.

Directionally frozen samples exhibit a variation in microstructure along their length. At the beginning of growth most samples contain a mixture of four-fold ferrite dendrites in a matrix composed of ferrite and titanate plate (Fig. 10). As freezing proceeds, the volume fraction of dendrites decreases leaving a plate-like aggregation of the two phases (Fig. 11). The form of the dendrites suggests that ⟨1 0 0⟩ ferrite direction lies along the solidification axis, as Boomgaard *et al.* [11] found for the spinel (and perovskite) phase in the $Co(Fe, Ti)_2O_4$–$BaTiO_3$ system. However, unlike their results we saw no evidence for a magneto-plumbite phase or for extensive solid

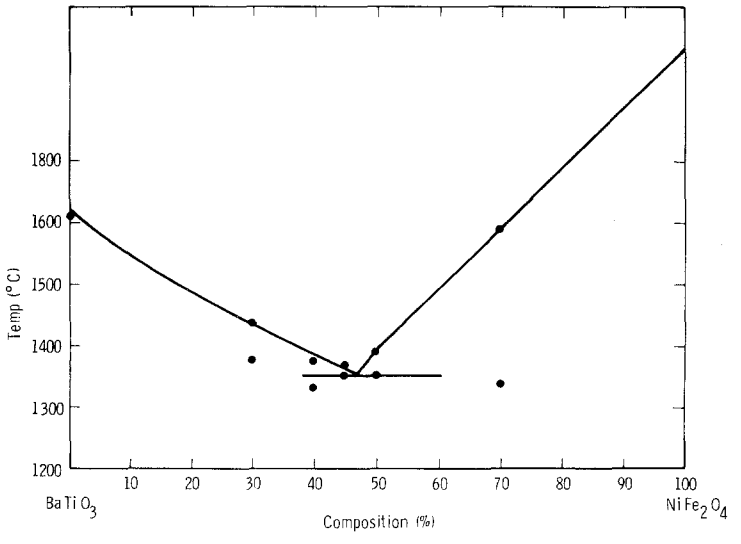

Figure 9 Partial phase diagram for the system $NiFe_2O_4$–$BaTiO_3$.

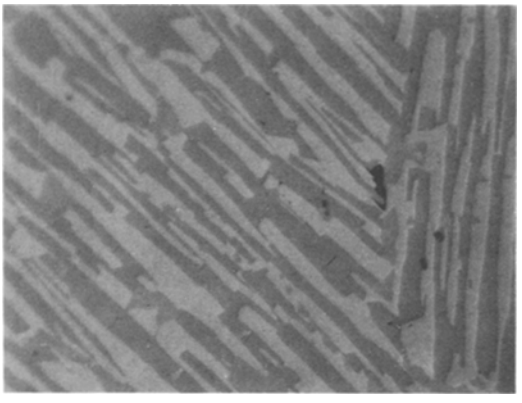

Figure 11 Faceted-lamellar structure in a directionally frozen nickel ferrite–barium titanate composite specimen. Transverse section × 262.5

solution in the ferrite phase. All our samples were frozen at 1 atm pressure in air; no attempt was made to assess the influence of gas pressure on specimen microstructure.

Of the three systems evaluated, the ferrite–titanate composites showed the least proclivity toward cracking, a result probably stemming from the crystallographic alignment of the phases [11] and close matching of their thermal expansion coefficients.

It can be concluded that the lithium ferrite–lithium niobate and lithium ferrite–lithium tantalate systems behave as pseudobinary eutectics and can be directionally frozen to form *in situ* composites comprised of a ferromagnetic and a piezoelectric phase. The microstructures are well behaved, with plate size decreasing as freezing rate increases in agreement with the well-documented relationship, $\lambda = AR^{-1/2}$ for other eutectic systems. For the niobate system a plate to rod transition apparently exists to higher growth rates. The tantalate system, on the other hand, exhibits features like a classic metal lamellar composite system: lamellar faults, fault lines, and breakdown to colony microstructure at rapid freezing rates.

The minimum melting composition on the $NiFe_2O_4$–$BaTiO_3$ join apparently does not represent an eutectic point as might be anticipated from the work of Van den Boomgaard *et al.* [11]. Instead, the composition plane is a cut through a melting trough in the system. Compositions on this trough when frozen produce initially dendritic microstructures containing a primary ferrite (spinel) phase. With continued freezing the liquid composition shifts until composite microstructures of the spinel and perovskite phases develop.

References

1. A. V. STEPANOV, *Bull. Acad. Sci. (USSR)* **33** (1969) 1775.
2. F. H. COCKS, J. T. A. POLLOCK and J. S. BULEY, Proceedings of the Conference on In Situ Composites, National Academy of Sciences, NMAB 308-I, Vol 1 (1973) p. 141.
3. T. F. CISZEK and G. H. SCHWUTTKE, *Phys. Stat. Sol.* (a)**27** (1975) 231.
4. H. E. LABELLE and A. I. MLAVSKY, *Mat. Res. Bull.* **6** (1971) 571.
5. National Bureau of Standards, Mono 25, Sec. 6 (1968) p. 22.
6. J. SHIEBER, *Inor. Nucl. Chem.* **26** (1964) 1363.
7. A. V. LAPICKIS and B. A. SIMANOV, *Zurnal fizic, Khimil* **29** (1955) 1201.
8. H. W. WEART and J. D. MACK, *Trans. Met. Soc. AIME* **212** (1958) 644.
9. SWANSON and FUYAT, NBS Circular 539, Vol. 10 (1953) p.44.
10. National Bureau of Standards (U.S.), Rep. 6415 (1959) p. 23.
11. J. VAN DEN BOOMGAARD, D. R. TEWELL, R. A. J. BORN and H. F. J. T. GELLER, *J. Mater. Sci.* **9** (1974) 1705.

Received 21 July
and accepted 27 August 1976

W. E. KRAMER
R. H. HOPKINS
MICHAEL R. DANIEL
Westinghouse Research Laboratories,
Pittsburgh,
Pennsylvania, USA